# Lamina cribrosa shape in non-human primates is different from that of humans

Miriam Bohlmann Kunz [1, †], Ziyi Zhu [1, †], Susannah Waxman [1], Bo Wang [1, 2, 3], Jacob Wallace [2], Samantha E. Schmitt [1, 4], Hiroshi Ishikawa [5, 6], Joel S. Schuman [1,2,7-10], Matthew A. Smith [1, 4, 11], Gadi Wollstein [7], Ian A. Sigal [1, 2 *]

1. Department of Ophthalmology, University of Pittsburgh, Pittsburgh, PA, USA
2. Department of Bioengineering, Swanson School of Engineering, University of Pittsburgh, Pittsburgh, PA, USA
3. Wilmer Eye Institute, Johns Hopkins University School of Medicine, Baltimore, MD, USA
4. Department of Biomedical Engineering, Carnegie Mellon University, Pittsburgh, PA, USA
5. Department of Ophthalmology, Casey Eye Institute, Oregon Health and Science University, Portland, OR, USA
6. Department of Medical Informatics and Clinical Epidemiology (DMICE), Oregon Health & Science University, Portland, OR, USA
7. Glaucoma Service, Wills Eye Hospital, Philadelphia, PA, USA
8. Vickie and Jack Farber Vision Research Center, Wills Eye Hospital, Philadelphia, PA, USA
9. School of Biomedical Engineering, Science and Health Studies, Drexel University, Philadelphia, PA, USA
10. Sidney Kimmel Medical College, Thomas Jefferson University, Philadelphia, PA, USA
11. Neuroscience Institute, Carnegie Mellon University, Pittsburgh, PA, USA

† - Both MB Kunz and Z Zhu should be considered first authors

**Short Title**: NHP LC shape

*** Correspondence:**
Ian A. Sigal, Ph.D., FARVO
Laboratory of Ocular Biomechanics
Department of Ophthalmology, University of Pittsburgh Medical Center,
1622 Locust St., Pittsburgh, PA, USA. 15219
Email: ian@OcularBiomechanics.com www.OcularBiomechanics.org

**Keywords**: Optic Nerve Head, Lamina Cribrosa, OCT, Intraocular Pressure, Intracranial Pressure, Translaminar pressure, Glaucoma, Biomechanics

**Proprietary Interest**: J.S. Schuman: JS Schuman: AEYE Health: C,PS; Alcon: C; Boehringer Ingelheim: C; BrightFocus: S; Carl Zeiss Meditec: C; NEI: S; Ocugenix: C,SO,PS,P; Ocular Therapeutics: C,US; Opticient: C,SO,PS; Perfuse: C,S; Regeneron: C; Slack: P; Tarsus: US; Tufts University School of Medicine: P; University of Pittsburgh Medical Center: P.
All other authors: Nothing to disclose.

**Financial support**: National Institutes of Health grants R01EY025011, R01EY013178, R01EY023966, R01EY028662, T32-EY017271 and P30EY008098; Glaucoma Research Foundation Shaffer Grant; Eye and Ear Foundation of Pittsburgh, PA; Research to Prevent Blindness (Unrestricted grants to UPMC Ophthalmology and NYU and Stein Innovation Award to Sigal IA).

**Word count**: 3405

**Accepted by Experimental Eye Research on 14 Oct 2025**

# Abstract

Non-human primates (NHPs) are a crucial model for studying glaucoma because of their similarities to humans in anatomy, physiology and pathology. Our goal in this study was to quantify in vivo NHP lamina cribrosa (LC) shapes at low, normal, and elevated intraocular pressures (IOPs), and compare them with literature reported values for in vivo human LCs. We imaged the optic nerve heads (ONH) of seven eyes from six rhesus macaque monkeys using spectral-domain optical coherence tomography (SD-OCT) at several IOP levels while keeping intracranial pressure at baseline. LC shape was characterized by measuring shape index (SI) and curvedness from manually delineated marks of the anterior LC surface. We found that LC shape in NHPs was more similar across individuals at normal IOP than it is in humans. This was, in part, because the NHPs LCs did not exhibit the characteristic horizontal central ridge seen in human LCs and were instead less saddle-shaped and more trough-shaped. With increasing IOP, NHPs LCs curvedness increased, without significant changes in SI, differing from the human response where SI decreases. These findings emphasize the importance of characterizing species-specific differences in anatomy and biomechanics, and the need to determine how these differences may impact susceptibility to glaucomatous damage.

The lamina cribrosa (LC) is a crucial structure within the optic nerve head (ONH) that provides structural support for retinal ganglion cell axons as they exit the eye and form the optic nerve.(Burgoyne, Downs et al. 2005, Furlanetto, Park et al. 2013) Numerous studies have documented a relationship between glaucoma and LC shape.(Kim, Jeoung et al. 2016, Tun, Thakku et al. 2016, Lee, Kim et al. 2017) For instance, glaucomatous damage to neural tissue is closely linked to a thinner LC and posterior bowing.(Quigley, Hohman et al. 1983) Although the exact mechanisms linking LC shape to glaucoma are not fully understood, the prevailing explanation is biomechanical: increased sensitivity to intraocular pressure (IOP) may heighten susceptibility to glaucoma, even at normal IOP levels.(Sigal and Ethier 2009, Stowell, Burgoyne et al. 2017) Thus, LC characteristics such as being thinner,(Quigley, Hohman et al. 1983, Jonas, Berenshtein et al. 2003, Jonas, Hayreh et al. 2011) increased bowing,(Quigley, Hohman et al. 1983) thinner beams,(Tezel, Trinkaus et al. 2004, Wang, Lucy et al. 2016) and a reduced density may contribute to mechanical fragility,(Albon, Purslow et al. 2000, Sigal, Flanagan et al. 2005, Yang, Downs et al. 2009) and consequently, a higher risk of glaucoma. LC shape has therefore emerged as an important biomechanical parameter, and most importantly as a potential biomarker for both glaucoma susceptibility and progression.(Lee, Kim et al. 2017) However, much remains to be learned about LC shape and its role in physiology and disease.

Due to their anatomical, physiological, and pathological similarities to humans, non-human primates (NHP) have become a crucial model for studying glaucoma.(Burgoyne 2015, Nguyen and Ethier 2015) The NHP LC is often regarded as the closest approximation to the human LC. Consequently, understanding how the LC in NHPs compares with that of humans, both in baseline shape and in response to changes in IOP, is increasingly important. In this study we aimed to quantify in vivo NHP LC shapes at low, normal, and elevated IOPs and compare them with reported values for human LCs. This comparison is crucial for accurately interpreting the NHP model of glaucoma and its relevance to human patients. The strengths of this study include: i) in vivo analysis, which, while more common now due to OCT advancements, contrasts with much of the existing LC knowledge derived from histology; ii) the use of intrinsic parameters to quantify LC shape, avoiding potential artifacts associated with older measures like depth,

which are defined relative to other structures; and iii) the control of both intraocular and intracranial pressure (ICP), acknowledging that both pressures can influence LC shape in complex ways.(Morgan, Chauhan et al. 2002, Zhao, He et al. 2015, Wang, Tran et al. 2017, Hua, Voorhees et al. 2018, Zhu, Waxman et al. 2021) For this study, we carefully varied IOP while maintaining ICP at a constant baseline level.

We utilized healthy, adult rhesus macaque monkeys as a model for our in vivo experiments. Surgical procedures, pressure control and imaging were as described before.(Zhu, Waxman et al. 2021) For clarity we will describe the key elements here. Both IOP and ICP were independently controlled to allow for simultaneous, acute manipulation. Seven eyes from six NHPs were imaged, in vivo, with optical coherence tomography (OCT) at four different IOPs. Each OCT image volume was processed into virtual radial slices on which ONH structures were manually delineated. Image processing was completed in FIJI.(Schindelin, Arganda-Carreras et al. 2012) Custom scripts were used to compute ALC curvedness and shape index (SI) from the delineations.

All animal procedures followed the National Institute of Health (NIH) Guide for the Care and Use of Laboratory Animals, adhered to the Association of Research in Vision and Ophthalmology (ARVO) statement for the Use of Animals in Ophthalmic and Vision Research, and were in accord with a protocol approved by the Institutional Animal Care and Use Committee (IACUC) of the University of Pittsburgh. Before the experiment, a clinical examination was conducted to exclude eyes with gross abnormality. Each of 6 NHPs were prepared for imaging as described previously.(Zhu, Waxman et al. 2021) Animals were initially sedated with 20 mg/kg ketamine, 1 mg/kg diazepam, and 0.04 mg/kg atropine. They were maintained on 1-3% isoflurane for the remainder of the experiment. Animals were placed on a ventilator and given vecuronium bromide, a paralytic, intravenously at 0.04-0.1 mg/kg/hour to reduce drift in eye position throughout the experiment. Pupils were dilated using tropicamide ophthalmic solution 0.5% (Bausch & Lomb, Rochester, NY). Eyes were scanned while animals were in the prone position, with the head held upright and facing the OCT device. The corneal surface of each eye was covered with a rigid, gas permeable contact lens (Boston EO, Boston, MA) to preserve corneal hydration and improve image quality. The eyes were kept open using a

wire speculum and the corneas were hydrated with saline between scans. The animals' blood pressures and heart rates were monitored throughout the study.

To control IOP, a 27-gauge needle was inserted into the anterior chamber and connected to a saline reservoir. To control ICP, a lumbar drain catheter was flushed of air, inserted 2.5 cm into the lateral ventricle of the brain, and then connected to a saline reservoir. The IOP was determined by the height of the reservoir. The ICP was determined by a pressure recorder placed into the lateral ventricle, at least 5 mm away from the catheter (Codman ICP Express, Johnson & Johnson, Raynham, MA). Before using the pressure transducer, it was calibrated while submerged in saline solution. IOP and ICP values were controlled within 1 mmHg. This study included 4 IOP conditions: low, normal, high, and very high. The target levels for each pressure group were 5, 15, 30, and 45 mmHg, while ICP was left at baseline (8-10 mmHg).(Suzuki, Iwase et al. 2006)

NHP eyes were imaged using spectral domain optical coherence tomography (SD-OCT, Bioptigen, Research Triangle, NC) with a scan rate of 20,000 A-scans/second, modified with a broadband superluminescent diode (Superlum, Dublin, Ireland, $\lambda = 870$ nm, $\Delta\lambda = 200$ nm). OCT scans were centered on the ONH region with a size of either 3x3x2 mm or 5x5x2 mm and 512x512x1024 pixels sampling. Under each pressure condition, multiple scans were taken and scans with the best quality were used to perform manual delineation. Image quality criteria are detailed previously.(Wang, Tran et al. 2017) After each pressure modulation, a minimum of 5 minutes wait time was allowed before imaging to ensure that viscoelastic effects had dissipated. In addition, at each pressure we spent 20-30 minutes adjusting equipment and conducting the imaging. Image quality tended to decrease with increasing anesthesia time. To ensure that image quality remained high, we imaged only one eye from most animals (5 out of 6). All scans were re-sampled at 1 x 1 x 1 scale for analysis.(Sigal, Schuman et al. 2016) Eyes vary in optical power and OCT systems are optimized for imaging human eyes. Hence, OCT images of NHP ONHs must be rescaled in the transverse dimensions. To set the dimensions, we followed the process described previously.(Wang, Tran et al. 2017) Briefly, after the experiment, eyes were enucleated, processed for cryosectioning, and sections were imaged with polarized light microscopy. The images were reconstructed into 3D stacks and used to obtain eye-specific transverse scaling factors based on the dimensions of the

scleral canal at Bruch's membrane opening (BMO). Elsewhere we have shown that this processing does not alter the scale of eye tissues.(Tran, Jan et al. 2017, Wang, Tran et al. 2017) The determined scaling factors were then applied to the OCT images before the following analysis.

We identified motion artifacts due to breathing and heartbeat as periodic patterns in the smooth structure of the Bruch's membrane in the OCT slow scan direction. We mitigated these artifacts by translating individual B-scan images for each A-scan along the axial direction. This was done using a virtual B-scan through the sclera as far from the canal as possible. The translation was done using gating to remove artifacts from breathing and heartbeat while preserving larger scale curvature. Preliminary markings were made on the BMO in the en face view to determine the BMO center (**Figure 1a**). Radial re-slicing from the BMO center was then performed on the OCT image volume using previously developed scripts in FIJI.(Wang, Tran et al. 2017) Through the re-slice process, we obtained 180 virtual, radial slices for each image volume (**Figure 1b**). A Gaussian filter was applied to the radial image stack before delineation of ONH features to remove the background noise and improve image quality.

Delineation of BMO and ALC in these radial slices was performed in FIJI by an experienced observer masked to IOP conditions. The delineation process yielded 3D markings of these ONH structures (**Figure 1c**), as is standard in studies of ONH morphology based on OCT.(Strouthidis, Fortune et al. 2011) We computed a measure of LC visibility by comparing the area of the ALC with the area of the scleral canal at the BMO. In this case we did the comparison at baseline IOP and ICP. The result was that global LC visibility was between 88 and 111%. This was possible because the BMO represents the narrowest point in the canal, widening posteriorly.

Delineations were imported from FIJI to MATLAB, where 3D ALC surfaces were reconstructed using scattered data interpolation. A confidence map was also imposed based on the markings distance to the interpolation so that we could focus analysis on regions with high reliability. The approach was similar to the conventional techniques used to detect outliers on one-dimensional function fits, but based on the distance from markings to a smooth delineation.

The scleral canal opening, defined as the best-fit plane of the BMO, was used as a reference plane for alignment, but it is important to note that the measurements analyzed did not depend on this reference (**Figure 1**).

The lamina cribrosa global shape index (SI, **Figure 1i**) introduced by Thakku et al,(Thakku, Tham et al. 2015) is a novel parameter to characterize the shape of the lamina cribrosa based on surface shape and curvature.(Koenderink and Van Doorn 1992) We computed the principal curvatures K1 and K2, which are the maximum and minimum curvature of the ALC surface among the 180 arcs (**Figure 1g**). Positive curvedness indicates a more posteriorly curved ALC while negative curvedness indicates a more anteriorly curved ALC. The SI and the curvedness are given by the formulas provided in **Figure 1g**. Reproducibility of LC delineations was demonstrated in an earlier publication,(Tran, Wallace et al. 2018) where we found values of 0.03 and 1.1x10-5 μm-1 for SI and curvedness, respectively.

When describing parameter changes, we defined positive changes as increase and negative changes as decrease, regardless of the parameter's value being positive or negative. For example, a positive change of a negatively valued parameter still indicates an increment toward positive infinity.

The shape index and curvedness were fit with linear fixed effect models. In the first model IOP was the fixed effect and NHP and eye were random effects. In the second model, eye was the fixed effect and NHP was the random effect. A p-value of 0.05 was the threshold for determining statistical significance.

The average ± standard deviation values for the LC SI and curvedness at baseline IOP were -0.81 ±0.08 and 33 ± 12 $10^{-5}$ $\mu m^{-1}$ respectively (**Figure 1k**). There was little variability in the SI across eyes and NHPs, whereas there was large variability in the curvedness.

The SI distribution of NHP eyes versus human eyes is shown in **Figure 1j** and **Figure 2g**. The ALC SI of NHPs measured in this study was between -0.9 and -0.6, which corresponds to shapes between rut and cup. In human subjects, however, most SIs were distributed between -0.7 and zero. (Thakku, Tham et al. 2015) This difference was due to the absence of the central ridge in the NHP eyes, which forms a characteristic saddle shape in human ALC.

Using a mixed effect model to fit the response of SI to increased IOP, there was no correlation between IOP and SI (**Figure 2b,c**). In addition, there was no correlation between eye and SI. We do see a positive correlation with IOP and changes in curvedness (**Figure 2e,f**).

The change plotted for SI and curvedness (**Figure 2a,d**) are the difference between the property value at baseline IOP (15 mmHg) and the property value at the new IOP. SI values did not vary much with IOP. The most significant change in curvedness was when increasing from low IOP to baseline IOP. The curvedness is lower at low IOP, meaning the ALC is flatter when the IOP is lower.Our goal with this study was to quantify the shape of in vivo NHP LCs at normal and elevated IOPs and to compare with reported values for in vivo human LCs. Three main findings emerged from our analysis. First, the LC SI at normal IOP in NHPs differed significantly from that in humans. Second, the variation in LC SI among NHPs was much smaller than in humans. Third, when IOP was higher than normal in NHPs, the LC became more curved, but its overall SI remained consistent, simply becoming a more exaggerated trough shape. In contrast, in human eyes with primary open angle glaucoma, the hypertensive IOP altered the LC shape more fundamentally, with the ridge flattening out, transforming the shape from a saddle-rut to a trough,(Kim, Jeoung et al. 2016, Lee, Kim et al. 2017) and in normal humans eyes the LC SI also decreased.(Tun, Thakku et al. 2016) Below we discuss these findings in more detail.

Based on the eyes imaged in this work, the average SI of NHP LCs at normal IOP was -0.81, corresponding with a trough-like shape. This shape is different from what has been reported for human LCs, which are typically saddle-shaped with a horizontal (nasal-temporal) ridge in the middle.(Thakku, Tham et al. 2015) NHPs are a common animal model for glaucoma. We note that even though each LC and sclera is unique in its microstructure, which therefore results in unique scleral compliance and LC material properties, the macroscopic property of SI had little variation across NHP eyes in this study. In addition, even though LC microstructure and material properties can change with increased IOP, the changes in these properties did not result in changes in SI with IOP.

From this study alone it is not clear if or how the different LC shapes will affect the LC biomechanics, including the sensitivity to IOP and susceptibility to glaucoma in NHPs when compared to humans. Potentially, the difference in shape could affect where axonal damage first occurs in the LC. In humans, axon damage has been shown to be focused in the superior and inferior regions of the LC.(Quigley and Addicks 1981, Azuara-Blanco, Costa et al. 2001, Lisboa, Leite et al. 2012) Axon damage in the NHP experimental glaucoma is more diffuse,(Quigley and Anderson 1977, Burgoyne and Morrison 2001) which could be at least partially due to the more symmetric trough shape of the LC in NHPs.

The variation in the LC SI was different in NHPs than has been reported for humans. The variation in SI for the NHP LCs was very small in contrast to the much more highly varied shapes reported of the human LC (**Figure 1j**). One possibility for the difference in variability between our results in NHPs and reports in humans is our measurements were made at constant ICP, while the ICP cannot be controlled in human patients. Both IOP and ICP are known to affect the LC position and shape.(Tran, Grimm et al. 2017, Hua, Voorhees et al. 2018) From the equations in Figure 1 readers should notice that curvedness depends on the ocular dimensions, whereas SI does not. SI is a measure of shape and was therefore selected to be independent of scale or size. Hence, it is fair to compare SI between eyes and species even if they have different overall sizes, whereas curvedness must be interpreted in the context of the scale.

When IOP was increased in NHPs the LC became more curved, but its overall shape measured by SI remained consistent, simply becoming more exaggerated. In contrast, in humans, increased IOP altered the LC shape more fundamentally, with the ridge flattening out, transforming the shape from a saddle to a trough.(Tun, Thakku et al. 2016) This difference in LC response to acute IOP increases between NHP and humans also hints at the different regional RGC death in glaucoma between NHP and human. (Burgoyne 2011)Perhaps in NHPs, that there is no preferential region of RGC death is partially due to the lack of extreme change in SI, but in humans the superior and inferior LC regions suffer more marked shape changes. Nevertheless, the exact implications of the difference in LC shape, variation, and response to IOP between NHPs and humans on glaucoma susceptibility remain to be determined.

In this study we have shown that there are differences between NHP and human LCs, but this does not imply that the NHP model for glaucoma is not a good model. The NHP experimental glaucoma model has proven extremely valuable to study LC biomechanics, and our results show there are differences between NHP and human LC anatomy that we must be aware of when interpreting NHP model results. No model is perfect, and it is essential to be aware of its limitations.

One advantage of the NHP model utilized in this study was the ability to control IOP and ICP separately, which is not possible when imaging human patients. These measurements of LC SI and curvedness were all made at variable IOP but constant ICP between all animals. Therefore, these results represent the impact only of IOP on LC shape. In addition, all these measurements were made in vivo and thus represent the intrinsic shape of the LC for each condition, and measurements of the same LC could be made at different IOP conditions. With histological methods, the LC must be sectioned to fully measure its shape, and the shape can only be measured at one condition.

Although we observed very little variation of LC shape in our sample size of seven eyes, a greater sample size would allow us to more definitively state whether there is any correlation between SI/curvedness and IOP. In addition, the implications of the LC differences between human and NHP on the susceptibility to glaucoma remain to be determined.

Another worthwhile consideration is some important aspects of LC shape and deformation likely occur in the LC interior, and not necessarily at the surface. The LC surface may sometimes be a good surrogate for the interior and sometimes it may not.(Sigal, Flanagan et al. 2004, Voorhees, Jan et al. 2017, Wei, Hua et al. 2022)

In addition to the differences in LC SI and curvedness, human and NHPs differ in other ways. For instance, compared with NHPs, human eyes are larger, with thicker LCs that are located more deeply within a scleral canal that is larger and rounder, and surrounded by a thicker sclera.(Sing, Anderson et al. 2000, Sanfilippo, Cardini et al. 2009, Sigal, Flanagan et al. 2010, Lockwood, Reynaud et al. 2015) Predicting the implications of these differences is extremely challenging due to their complex nonlinear interactions.(Hua, Voorhees et al. 2018, Zhu, Waxman et al. 2021) For example, while increased thickness and material stiffness individually reduce sensitivity to elevated IOP,

their combined effects do not follow a simple additive pattern. Instead, sensitivity to thickness decreases in stiff tissues and sensitivity to stiffness decreases in compliant tissues. Interested readers can consult reports on the use of computational parametric modeling that explore the sensitivity of ONH biomechanics to these parameters, both independently and together.(Hua, Voorhees et al. 2020, Schwaner, Feola et al. 2020, Liu, Hung et al. 2024, Otani, Miyata et al. 2024)

In conclusion, we aimed to explore the interaction between IOP and LC shape in a NHP model and compare these results to those in humans. We demonstrate that NHP LC shape has little variation across animals, the LC shape is trough-like, and the LC shape does not change with IOP, only the curvedness. These results of NHP LC shape are all in contrast to human LCs, which are varied in shape, typically have a nasal-temporal rut, and change shape with an increase in IOP. As NHPs are a common model to study LC biomechanics, these results show that there are differences between the NHP model and humans that must be considered.

# Figures

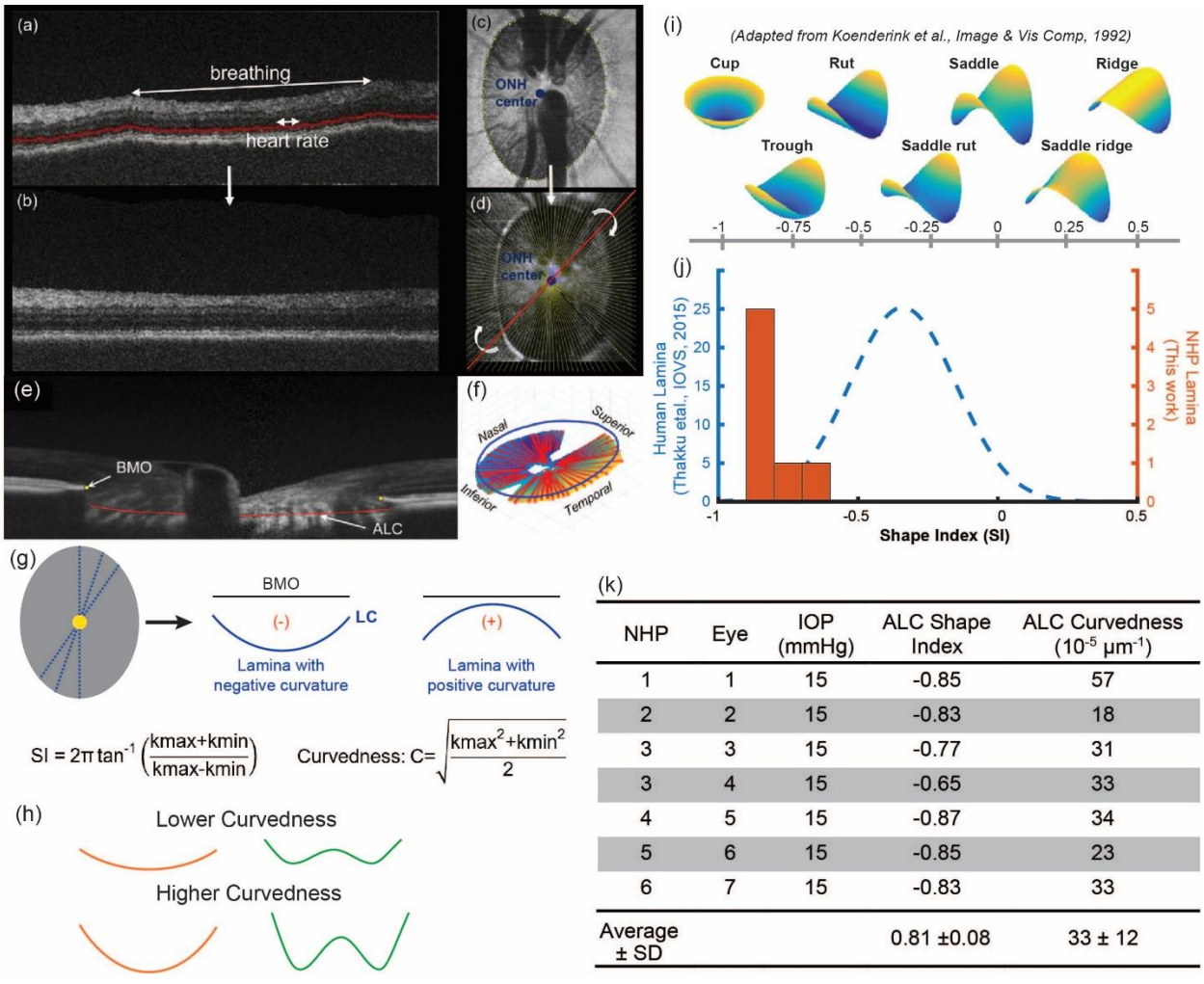


(k)

| NHP | Eye | IOP (mmHg) | ALC Shape Index | ALC Curvedness ($10^{-5}$ µm$^{-1}$) |
|---|---|---|---|---|
| 1 | 1 | 15 | -0.85 | 57 |
| 2 | 2 | 15 | -0.83 | 18 |
| 3 | 3 | 15 | -0.77 | 31 |
| 3 | 4 | 15 | -0.65 | 33 |
| 4 | 5 | 15 | -0.87 | 34 |
| 5 | 6 | 15 | -0.85 | 23 |
| 6 | 7 | 15 | -0.83 | 33 |
| Average ± SD | | | 0.81 ±0.08 | 33 ± 12 |

Figure 1. (a) An original orthogonal slice with motion artifacts outlined by manual marking (red) of Bruch membrane layer and (b) after motion artifacts removed. (c) En-face view of BMO outline (yellow dots) used to determine ONH center (blue) for radial re-slicing (d). The sample radial lines intersect at the ONH center and were generated in a counterclockwise sequence (red). An example virtual radial OCT slice (e) with manual delineations of the BMO (yellow) and ALC (red), and the ALC delineations are reconstructed to create a heat map of the ALC surface (f), with shallower to deeper: blue to red. (g, left) Points from each ALC surface are sample radially every 1 degree, centered at the centroid of the scleral canal. (g, right) These points are fitted to circles with negative (positive) curvature corresponding with a concave (convex) LC shape. Definitions of SI and curvedness, calculated from the principal curvatures (kmax, kmin). (h) Illustrations of lower versus higher surface curvedness (orange, green) having the same SI. (i) Illustration of surfaces (shallower to deeper: yellow to blue) with SI ranging from a cup to a ridge. (j) NHP (red) vs. human (blue) LC SI at normal IOP, and (k) SI and curvedness values for all NHP eyes used in this study.

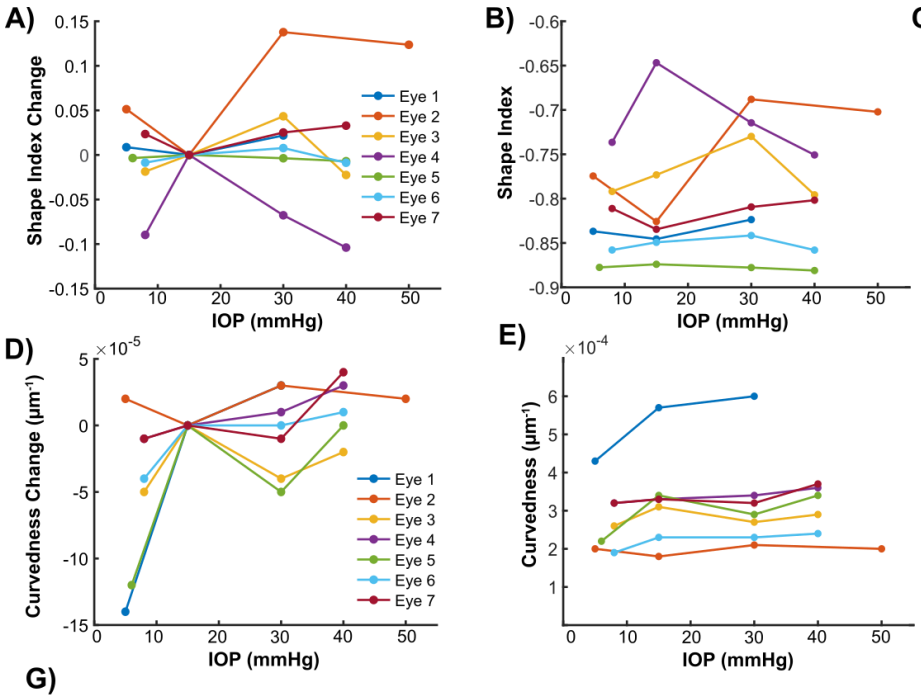


**C)**

**Shape Index**

| | $\beta(10^{-3})$ | $p$ |
|---|---|---|
| **Eye** | 4 | 0.75 |
| **IOP** | 0.5 | 0.25 |

**F)**

**Curvedness**

| | $\beta(10^{-6})$ | $p$ |
|---|---|---|
| **Eye** | 15 | 0.47 |
| **IOP** | 1.3 | 0.018* |

**significant p<0.05*

**G)**

| | | IOP Levels | | | |
|---|---|---|---|---|---|
| | | *Low* | *Baseline* | *High* | *Very High* |
| **Human** | *IOP (mmHg)* | -- | 17 ± 3 | 38 ± 6 | 46 ± 6 |
| *(Tun et al., IOVS, 2016)* | *Shape Index* | -- | -0.21 ± 0.19 | -0.29 ± 0.21 | -0.27 ± 0.2 |
| **NHP** | *IOP (mmHg)* | 7 ± 1 | 15 | 30 | 42 ± 4 |
| | *Shape Index* | -0.81 ± 0.05 | -0.81 ± 0.1 | -0.78 ± 0.1 | -0.8 ± 0.1 |

Figure 2: (a) Changes in individual lamina SI and (d) curvedness at low, baseline, and hypertensive IOPs for seven NHP eyes. The change is the change in property compared to the value at baseline IOP, therefore the change at baseline is zero. The raw values of SI and curvedness for the 7 NHP eyes are plotted in (b) and (e). It is important to note that we only had data at the four IOP levels specified. In the plots we connected the dots with straight lines, but this was only done for clarity and not to imply that the relationship between IOP and SI or curvedness was linear in the range. The starting IOP is different for each eye as lowering the IOP past a threshold would lead to corneal buckling and clouding. The threshold was different for each eye. Mixed effect models were fit to SI and curvedness (c) and (f) respectively. These fits show that there is no linear relationship between IOP and SI, but there is a significant relationship between IOP and curvedness. (g) The SI values of human and NHPs at various IOPs. We observe a consistent SI in NHP LCs that is lower than in human LCs, that does not change with an increase in IOP.

# References


Albon, J., P. P. Purslow, W. S. Karwatowski and D. L. Easty (2000). "Age related compliance of the lamina cribrosa in human eyes." British Journal of Ophthalmology 84(3): 318-323.

Azuara-Blanco, A., V. P. Costa and R. P. Wilson (2001). Handbook of glaucoma. London, Taylor & Francis Group.

Burgoyne, C. F. (2011). "A biomechanical paradigm for axonal insult within the optic nerve head in aging and glaucoma." Experimental eye research 93(2): 120-132.

Burgoyne, C. F. (2015). "The non-human primate experimental glaucoma model." Experimental eye research 141: 57-73.

Burgoyne, C. F., J. C. Downs, A. J. Bellezza, J. K. Suh and R. T. Hart (2005). "The optic nerve head as a biomechanical structure: a new paradigm for understanding the role of IOP-related stress and strain in the pathophysiology of glaucomatous optic nerve head damage." Prog Retin Eye Res 24(1): 39-73.

Burgoyne, C. F. and J. C. Morrison (2001). "The anatomy and pathophysiology of the optic nerve head in glaucoma." Journal of glaucoma 10(5): S16-S18.

Furlanetto, R. L., S. C. Park, U. J. Damle, S. F. Sieminski, Y. Kung, N. Siegal, J. M. Liebmann and R. Ritch (2013). "Posterior displacement of the lamina cribrosa in glaucoma: in vivo interindividual and intereye comparisons." Invest Ophthalmol Vis Sci 54(7): 4836-4842.

Hua, Y., A. P. Voorhees, N. J. Jan, B. Wang, S. Waxman, J. S. Schuman and I. A. Sigal (2020). "Role of radially aligned scleral collagen fibers in optic nerve head biomechanics." Exp Eye Res 199: 108188.

Hua, Y., A. P. Voorhees and I. A. Sigal (2018). "Cerebrospinal fluid pressure: revisiting factors influencing optic nerve head biomechanics." Investigative ophthalmology & visual science 59(1): 154-165.

Jonas, J. B., E. Berenshtein and L. Holbach (2003). "Anatomic relationship between lamina cribrosa, intraocular space, and cerebrospinal fluid space." Investigative ophthalmology & visual science 44(12): 5189-5195.

Jonas, J. B., S. S. Hayreh and T. Yong (2011). "Thickness of the lamina cribrosa and peripapillary sclera in Rhesus monkeys with nonglaucomatous or glaucomatous optic neuropathy." Acta Ophthalmologica 89(5): e423-e427.

Kim, Y. W., J. W. Jeoung, D. W. Kim, M. J. Girard, J. M. Mari, K. H. Park and D. M. Kim (2016). "Clinical assessment of lamina cribrosa curvature in eyes with primary open-angle glaucoma." PloS one 11(3): e0150260.

Koenderink, J. J. and A. J. Van Doorn (1992). "Surface shape and curvature scales." Image and vision computing 10(8): 557-564.

Lee, S. H., T.-W. Kim, E. J. Lee, M. J. Girard and J. M. Mari (2017). "Diagnostic power of lamina cribrosa depth and curvature in glaucoma." Investigative ophthalmology & visual science 58(2): 755-762.

Lisboa, R., M. T. Leite, L. M. Zangwill, A. Tafreshi, R. N. Weinreb and F. A. Medeiros (2012). "Diagnosing preperimetric glaucoma with spectral domain optical coherence tomography." Ophthalmology 119(11): 2261-2269.

Liu, T., P. T. Hung, X. Wang and M. J. A. Girard (2024). "Effect of Eye Globe and Optic Nerve Morphologies on Gaze-Induced Optic Nerve Head Deformations." Invest Ophthalmol Vis Sci 65(8): 48.

Lockwood, H., J. Reynaud, S. Gardiner, J. Grimm, V. Libertiaux, J. C. Downs, H. Yang and C. F. Burgoyne (2015). "Lamina cribrosa microarchitecture in normal monkey eyes part 1: methods and initial results." Invest Ophthalmol Vis Sci 56(3): 1618-1637.

Morgan, W. H., B. C. Chauhan, D. Y. Yu, S. J. Cringle, V. A. Alder and P. H. House (2002). "Optic Disc Movement with Variations in Intraocular and Cerebrospinal Fluid Pressure." Invest Ophthalmol Vis Sci 43(10): 3236-3242.

Nguyen, T. D. and C. R. Ethier (2015). "Biomechanical assessment in models of glaucomatous optic neuropathy." Experimental eye research 141: 125-138.

Otani, T., K. Miyata, A. Miki and S. Wada (2024). "Computational study on the effects of central retinal blood vessels with asymmetric geometries on optic nerve head biomechanics." Med Eng Phys 123: 104086.

Quigley, H. and D. R. Anderson (1977). "Distribution of axonal transport blockade by acute intraocular pressure elevation in the primate optic nerve head." Investigative ophthalmology & visual science 16(7): 640-644.

Quigley, H. A. and E. M. Addicks (1981). "Regional Differences in the Structure of the Lamina Cribrosa and Their Relation to Glaucomatous Optic Nerve Damage." Archives of Ophthalmology 99(1): 137-143.

Quigley, H. A., R. M. Hohman, E. M. Addicks, R. W. Massof and W. R. Green (1983). "Morphologic changes in the lamina cribrosa correlated with neural loss in open-angle glaucoma." American Journal of Ophthalmology 95(5): 673-691.

Sanfilippo, P. G., A. Cardini, A. W. Hewitt, J. G. Crowston and D. A. Mackey (2009). "Optic disc morphology--rethinking shape." Prog Retin Eye Res 28(4): 227-248.

Schindelin, J., I. Arganda-Carreras, E. Frise, V. Kaynig, M. Longair, T. Pietzsch, S. Preibisch, C. Rueden, S. Saalfeld, B. Schmid, J.-Y. Tinevez, D. J. White, V. Hartenstein, K. Eliceiri, P. Tomancak and A. Cardona (2012). "Fiji: an open-source platform for biological-image analysis." Nat. Methods 9(7): 676-682.

Schwaner, S. A., A. J. Feola and C. R. Ethier (2020). "Factors affecting optic nerve head biomechanics in a rat model of glaucoma." J R Soc Interface 17(165): 20190695.

Sigal, I. A. and C. R. Ethier (2009). "Biomechanics of the optic nerve head." Exp Eye Res 88: 799-807.

Sigal, I. A., J. G. Flanagan and C. R. Ethier (2005). "Factors influencing optic nerve head biomechanics." Invest Ophthalmol Vis Sci 46(11): 4189-4199.

Sigal, I. A., J. G. Flanagan, I. Tertinegg and C. R. Ethier (2004). "Finite element modeling of optic nerve head biomechanics." Invest Ophthalmol Vis Sci 45(12): 4378-4387.

Sigal, I. A., J. G. Flanagan, I. Tertinegg and C. R. Ethier (2010). "3D morphometry of the human optic nerve head." Exp Eye Res 90(1): 70-80.

Sigal, I. A., J. S. Schuman, H. Ishikawa, L. Kagemann and G. Wollstein (2016). "A problem of proportions in OCT-based morphometry and a proposed solution." Investigative ophthalmology & visual science 57(2): 484-485.

Sing, N. M., S. F. Anderson and J. C. Townsend (2000). "The normal optic nerve head." Optom Vis Sci 77(6): 293-301.

Stowell, C., C. F. Burgoyne, E. R. Tamm, C. R. Ethier, I. I. o. A. Lasker and P. Glaucomatous Neurodegeneration (2017). "Biomechanical aspects of axonal damage in glaucoma: A brief review." Exp Eye Res 157: 13-19.

Strouthidis, N. G., B. Fortune, H. Yang, I. A. Sigal and C. F. Burgoyne (2011). "Effect of acute intraocular pressure elevation on the monkey optic nerve head as detected by spectral domain optical coherence tomography." Investigative ophthalmology & visual science 52(13): 9431-9437.

Suzuki, Y., A. Iwase, M. Araie, T. Yamamoto, H. Abe, S. Shirato, Y. Kuwayama, H. K. Mishima, H. Shimizu and G. Tomita (2006). "Risk factors for open-angle glaucoma in a Japanese population: the Tajimi Study." Ophthalmology 113(9): 1613-1617.

Tezel, G., K. Trinkaus and M. Wax (2004). "Alterations in the morphology of lamina cribrosa pores in glaucomatous eyes." British journal of ophthalmology 88(2): 251-256.

Thakku, S. G., Y.-C. Tham, M. Baskaran, J.-M. Mari, N. G. Strouthidis, T. Aung, C.-Y. Cheng and M. J. Girard (2015). "A global shape index to characterize anterior lamina cribrosa morphology and its determinants in healthy Indian eyes." Investigative ophthalmology & visual science 56(6): 3604-3614.

Tran, H., J. Grimm, B. Wang, M. Smith, A. Gogola, S. Nelson, E. Tyler-Kabara, J. Schuman, G. Wollstein and I. Sigal (2017). Mapping in-vivo optic nerve head strains caused by intraocular and intracranial pressures. Optical elastography and tissue biomechanics IV, SPIE.

Tran, H., N.-J. Jan, D. Hu, A. Voorhees, J. S. Schuman, M. A. Smith, G. Wollstein and I. A. Sigal (2017). "Formalin fixation and cryosectioning cause only minimal changes in shape or size of ocular tissues." Scientific reports 7(1): 12065.

Tran, H., J. Wallace, Z. Zhu, K. A. Lucy, A. P. Voorhees, S. E. Schmitt, R. A. Bilonick, J. S. Schuman, M. A. Smith and G. Wollstein (2018). "Seeing the hidden lamina: effects of exsanguination on the optic nerve head." Investigative Ophthalmology & Visual Science 59(6): 2564-2575.

Tun, T. A., S. G. Thakku, O. Png, M. Baskaran, H. M. Htoon, S. Sharma, M. E. Nongpiur, C.-Y. Cheng, T. Aung and N. G. Strouthidis (2016). "Shape changes of the anterior lamina cribrosa in normal, ocular hypertensive, and glaucomatous eyes following acute intraocular pressure elevation." Investigative ophthalmology & visual science 57(11): 4869-4877.

Voorhees, A. P., N. J. Jan, M. E. Austin, J. G. Flanagan, J. M. Sivak, R. A. Bilonick and I. A. Sigal (2017). "Lamina Cribrosa Pore Shape and Size as Predictors of Neural Tissue Mechanical Insult." Invest Ophthalmol Vis Sci 58(12): 5336-5346.

Wang, B., K. A. Lucy, J. S. Schuman, I. A. Sigal, R. A. Bilonick, L. Kagemann, T. Kostanyan, C. Lu, J. Liu and I. Grulkowski (2016). "Decreased lamina cribrosa beam thickness and pore diameter relative to distance from the central retinal vessel trunk." Investigative Ophthalmology & Visual Science 57(7): 3088-3092.

Wang, B., H. Tran, M. A. Smith, T. Kostanyan, S. E. Schmitt, R. A. Bilonick, N.-J. Jan, L. Kagemann, E. C. Tyler-Kabara and H. Ishikawa (2017). "In-vivo effects of intraocular and intracranial pressures on the lamina cribrosa microstructure." PloS one 12(11): e0188302.

Wei, J., Y. Hua, B. Yang, B. Wang, S. E. Schmitt, B. Wang, K. A. Lucy, H. Ishikawa, J. S. Schuman, M. A. Smith, G. Wollstein and I. A. Sigal (2022). "Comparing Acute IOP-

Induced Lamina Cribrosa Deformations Premortem and Postmortem." Transl Vis Sci Technol 11(12): 1.

Yang, H., J. C. Downs, I. A. Sigal, M. D. Roberts, H. Thompson and C. F. Burgoyne (2009). "Deformation of the normal monkey optic nerve head connective tissue after acute IOP elevation within 3-D histomorphometric reconstructions." Investigative ophthalmology & visual science 50(12): 5785-5799.

Zhao, D., Z. He, A. J. Vingrys, B. V. Bui and C. T. O. Nguyen (2015). "The effect of intraocular and intracranial pressure on retinal structure and function in rats." Physiological Reports 3(8): e12507.

Zhu, Z., S. Waxman, B. Wang, J. Wallace, S. E. Schmitt, E. Tyler-Kabara, H. Ishikawa, J. S. Schuman, M. A. Smith, G. Wollstein and I. A. Sigal (2021). "Interplay between intraocular and intracranial pressure effects on the optic nerve head in vivo." Exp. Eye Res. 213: 108809.